J. Phys. Earth, **34**, 335—355, 1986

FRACTURE ENERGY AND THE VARIATION OF GOUGE AND SURFACE ROUGHNESS DURING FRICTIONAL SLIDING OF ROCKS

Naoto YOSHIOKA

Information Processing Center, Yokohama City University, Yokohama, Japan

(Received November 2, 1985; Revised August 16, 1986)

Fracture energy was estimated on the basis of experimental results with respect to both the amount and the particle size distribution of the gouges which were developed during frictional slidings. The result shows that the fracture energy occupies only 0.01–0.1% in the total energy released by the testing machine: the heat energy due to friction and the elastic wave energy are the main two forms in the distribution process.

Nevertheless the gouge and the roughness of the sliding surface play an important role in the distribution process of energy. The energy budget during sliding depends upon the existence of gouge. In addition, gouge and surface roughness reflect the history of sliding or the sliding behaviour. It is useful to study the variation of gouge and surface roughness in experiments for investigating the earthquake source mechanism.

1. *Introduction*

The strain energy which is stored in the Earth is released when earthquakes occur. Through the dislocation process of the earthquakes, the released energy is converted to various forms of energy, that is, radiated seismic energy, fracture energy and frictional heat (HUSSEINI, 1977). The seismic efficiency η is the ratio of the radiated seismic energy to the total released energy. Therefore, when one discusses the seismic efficiency, it is necessary to estimate the distribution of the energy among the various forms. Some authors have attempted to estimate the energy distribution either by the analytical methods (e.g., KING, 1969; HUSSEINI, 1977), or by the experimental methods (e.g., SCHOLZ *et al.*, 1972; LOCKNER and OKUBO, 1983). SCHOLZ *et al.* (1972) discussed the seismic efficiency on the basis of the kinetic coefficient of friction and suggested that η increases with stress drop. LOCKNER and OKUBO (1983) directly measured the temperature rise due to friction and concluded that the seismic efficiency is 4–8%. However, both of them did not take the fracture energy into account. The frictional sliding always accompanies the ploughing of the sliding surfaces (ENGELDER, 1974) and subsequently produces gouge particles between the sliding surfaces, thus the fracture energy may occupy a

certain part in the total released energy. However, only a few attempts have been made to quantitatively estimate the fracture energy.

In previous papers (YOSHIOKA, 1984, 1985), we showed that the temperature measurement in experiments is an effective method for investigating the energy budget during sliding. The relation between the heat generation and the stress drop during frictional sliding of rocks was empirically found: the heat generation due to frictional sliding decreases as the fractional stress drop, which is a ratio of stress drop $\Delta\tau$ to the initial stress τ_1, increases. The empirical formula is given by $a = 1-\Delta\tau/\tau_1$, where a is the average magnitude of the heat sources on the sliding surface, which is also the ratio of the energy dissipated in the form of heat to the energy supplied by a testing machine.

The variations of gouge and surface roughness due to repeated frictional slidings were also observed throughout the experiments. In the present paper we first describe the methods and the results of the observations and estimate the fracture energy on the basis of the experimental results.

2. *Experimental Procedure*

Since the experimental procedure is fully described in the previous paper (YOSHIOKA, 1985), only a brief description will be given here. Using a bi-axial direct shear apparatus, we have conducted frictional sliding experiments on sandstone and granite. In a sliding run experiment, we first increased the normal load and kept it constant, then gradually applied the shear load. According to the normal stress level, various sliding modes appeared from stable sliding to violent stick-slip. Tables 1 a and b show the stress conditions and the results of all sliding runs.

As well as the normal and shear load and displacement, temperature rise due to frictional heating was measured by five thermistors buried in rock samples, the results from which were presented in the previous paper (YOSHIOKA, 1985). In series A experiments (Tables 1 a and b), we observed the amount and the particle size of gouge which was developed between fault surfaces. Further, we measured the variation in surface roughness by a profilometer after a removal of gouge. Unfortunately, we could not obtain, however, satisfactory data with respect to particle size distribution of gouge and surface roughness for the sandstone sample. Therefore we will mainly describe and discuss the results from the granite sample.

3. *Gouge*

A number of authors have reported the mechanical properties and the effects of gouges on the sliding behavior of rocks (OHNAKA, 1975; WU *et al.*, 1975; SUMMERS and BYERLEE, 1977; SHIMAMOTO, 1977; WANG *et al.*, 1980; SHIMAMOTO and LOGAN, 1981). Clay gouges are considered to be the products of faultings and to play an important role in the sliding behaviour of faults.

Table 1a. Conditions and results of the experiments on CHS-SS.

Series	Cycle	Run No.	σ (MPa)	τ (MPa)	D (cm)	t_1 (s)	A (cm^2)	Sliding mode	Gouge (mg/cm^2)
A	1	CHS-1	11.1	6.7	0.820	28.3	100.0	I	3.84
		CHS-2	11.6	7.0	0.770	11.2	96.0	I	3.44
		CHS-3	11.5	7.3	0.894	9.1	96.0	I	
		CHS-4	11.5	6.9	0.840	9.2	96.0	I	3.15
	2	CHS-5	7.1	4.4	0.922	10.3	96.0	I	
		CHS-6	7.1	4.1	0.894	10.6	96.0	I	2.09
		CHS-7	7.5	4.3	0.895	10.7	96.0	I	1.78
	3	CHS-8	3.7	2.1	0.948	10.5	96.0	I	
		CHS-9	3.7	2.0	0.813	9.3	96.0	I	1.49
		CHS-10	3.6	2.1	1.122	12.2	96.0	I	1.17
	4	CHS-11	17.0	10.6	1.050	12.0	96.0	I	
		CHS-12	16.9	10.3	0.705	9.0	96.0	I	3.87
		CHS-13	16.7	10.8	1.030	11.9	96.0	I	3.22
	5	CHS-14	23.7	13.7	0.882	9.2	96.0	I	
		CHS-15	22.9	13.1	0.772	8.1	96.0	I	4.13
		CHS-16	20.8	14.4	0.833	8.5	96.0	I	3.46
	6	CHS-17	31.4	20.1	0.989	10.9	65.0	I	
		CHS-18	30.3	19.6	0.885	9.2	65.0	I	12.3
		CHS-19	31.3	20.2	0.792	8.6	65.0	I	6.85
	7	CHS-20	35.6	24.1	0.916	11.0	65.0	I	
		CHS-21	35.0	22.4	0.799	12.1	65.0	I	11.4
		CHS-22	36.5	22.0	0.865	9.9	65.0	I	8.63
B		CHS-23	4.6	3.0	0.839	8.5	65.0	I	
		CHS-24	4.7	3.0	0.723	7.9	65.0	I	
		CHS-25	4.5	2.9	0.789	10.0	65.0	I	
		CHS-26	9.8	6.0	0.805	8.7	65.0	I	
		CHS-27	14.2	9.3	0.953	9.0	65.0	I	
		CHS-28	19.0	11.9	0.760	10.0	65.0	I	
		CHS-29	23.5	14.8	0.675	7.3	65.0	I	
		CHS-30	27.1	17.7	0.833	10.4	65.0	I	
		CHS-31	32.6	22.1	0.196	5.5	65.0	I	
		CHS-32	32.4	20.5	0.791	9.2	65.0	I	
		CHS-33	35.1	22.7	0.824	10.2	65.0	I	
		CHS-34	18.5	12.0	0.869	9.3	65.0	I	
		CHS-35	9.6	6.0	0.838	9.5	65.0	I	
		CHS-36	4.7	3.0	0.915	10.0	65.0	I	

σ, average normal stress; τ, average shear stress; D, displacement; t_1, duration time of slip; A, sliding surface area.

Table 1 b. Conditions and results of the experiments on MKB-GR.

Series	Cycle	Run No.	σ (MPa)	τ (MPa)	D (cm)	t_1 (s)	A (cm^2)	Sliding mode	Gouge (mg/cm^2)
A	1	MKB-1	8.3	5.4	0.914	10.1	40.0	II	
		MKB-2	8.5	5.5	0.971	10.8	40.0	II	0.350
		MKB-3	8.7	5.1	0.966	10.7	40.0	II	0.175
	2	MKB-4	17.1	9.5	0.932	10.6	40.0	II	
		MKB-5	16.9	10.3	0.858	9.9	40.0	II	0.350
		MKB-6	16.8	9.9	0.912	9.8	40.0	II	0.225
	3	MKB-7	25.9	15.4	0.753	12.3	40.0	II	
		MKB-8	25.0	16.7	0.834	11.4	40.0	II	1.25
		MKB-9	25.9	16.0	0.874	10.7	40.0	II	0.775
	4	MKB-10	32.3	20.9	0.853	14.1	40.0	II	
		MKB-11	31.6	22.1	0.917	11.9	40.0	II	2.58
		MKB-12	33.6	21.6	0.788	9.9	40.0	I	2.13
	5	MKB-13	42.8	26.8	0.887	10.3	40.0	II	
		MKB-14	41.5	26.8	0.863	12.2	40.0	I	4.78
		MKB-15	39.3	27.4	0.829	9.2	40.0	II	3.30
	6	MKB-16	54.4	35.5	0.901	12.0	40.0	II	
		MKB-17	52.9	36.2	1.165	13.4	40.0	I	8.85
		MKB-18	53.9	34.3	0.885	9.3	40.0	III	7.88
	7	MKB-19	63.7	37.3	1.189	12.4	40.0	III	
		MKB-20	66.5	42.6	1.155	15.6	40.0	I	15.1
		MKB-21	60.9	35.0	1.199	12.9	40.0	III	13.7
	8	MKB-22	71.5	33.3	1.350	14.3	40.0	IV	
		MKB-23	83.7	51.2	1.202	15.7	40.0	I	21.5
		MKB-24	70.3	32.8	1.517	16.2	40.0	IV	14.0
	9	MKB-25	86.0	48.0	1.419	15.9	24.4	III	
		MKB-26	100.7	61.7	1.099	15.3	24.4	I	30.2
		MKB-27	83.9	43.7	1.060	11.0	24.4	III	21.8
	10	MKB-28	101.4	67.0	1.134	13.6	24.4	II	
		MKB-29	99.0	62.1	1.011	11.4	24.4	I	34.8
		MKB-30	103.3	60.8	1.086	11.4	24.4	II	31.8
	11	MKB-31	101.2	51.7	1.269	13.6	24.4	III	
		MKB-32	110.0	69.2	0.926	11.1	24.4	I	48.2
		MKB-33	111.7	70.8	1.107	12.3	24.4	II	42.0
B		MKB-34	15.3	8.8	1.279	15.6	24.4	I	
		MKB-35	15.2	8.8	1.329	26.9	24.4	I	
		MKB-36	15.9	8.7	1.174	13.8	24.4	I	
		MKB-37	15.2	8.8	1.135	14.0	24.4	I	

Table 1 b. (continued)

Series	Cycle	Run No.	σ (MPa)	τ (MPa)	D (cm)	t_1 (s)	A (cm^2)	Sliding mode	Gouge (mg/cm^2)
		MKB-38	29.9	17.4	1.086	13.0	24.4	I	
		MKB-39	29.9	17.6	1.052	13.8	24.4	I	
		MKB-40	44.2	26.5	1.209	15.4	24.4	I	
		MKB-41	44.0	26.3	1.001	11.8	24.4	I	
		MKB-42	15.3	8.9	1.021	12.1	24.4	I	
		MKB-43	15.1	8.9	1.052	14.2	24.4	I	
		MKB-44	30.3	17.8	1.140	15.4	24.4	I	
		MKB-45	29.8	18.3	1.155	13.0	24.4	I	
		MKB-46	29.5	17.8	1.028	12.4	24.4	I	
		MKB-47	43.0	26.3	1.021	14.3	24.4	I	
		MKB-48	43.4	27.3	1.246	18.2	24.4	I	
B		MKB-49	58.3	34.0	1.001	13.5	24.4	I	
		MKB-50	58.1	36.3	1.104	15.1	24.4	I	
		MKB-51	70.9	45.2	1.129	15.8	24.4	I	
		MKB-52	70.9	44.8	1.080	14.4	24.4	I	
		MKB-53	80.7	54.7	1.132	15.7	24.4	I	
		MKB-54	83.2	55.5	1.255	16.3	24.4	I	
		MKB-55	92.1	67.8	1.082	14.8	24.4	I	
		MKB-56	96.1	59.0	1.028	15.4	24.4	I	
		MKB-57	95.0	65.8	0.935	13.4	24.4	I	
		MKB-58	104.9	75.3	1.062	14.2	24.4	I	
		MKB-59	107.5	76.0	1.067	14.0	24.4	I	
		MKB-60	90.6	62.6	0.965	12.1	24.4	I	

3.1 The amount of gouge

The amount of the gouge developed per unit area is shown in Figs. 1 (a) and (b) as a function of displacement. The data under the same initial stress condition are connected by the solid lines. Each line corresponds to a cycle in series A experiment. The numbers in the figure denote the initial normal stress σ_i immediately before the onset of sliding, which is different from the average normal stress σ during sliding because the reduction or the fluctuation occurred in the normal stress during sliding when the stick-slip took place.

The factors which affect the amount of gouge are considered to be (1) the strength of the intact rock, (2) the magnitude of displacement, (3) the normal stress, (4) the presence of gouge which already exists before sliding, and (5) the sliding mode.

The effect of the strength of the rock samples on the productivity of gouge can be seen in the difference of the rock materials. Figure 2 shows the amount of the gouge developed per unit sliding area at the same magnitude of displacement (1.5 cm) as a function of the initial normal stress, which is inferred from Fig. 1. The slidings of the Choshi sandstone (CHS-SS) produced a larger amount of gouge than those of Makabe granite (MKB-GR) if the other conditions such as the normal stress and the magnitude of displacement are the same. The uniaxial compressive

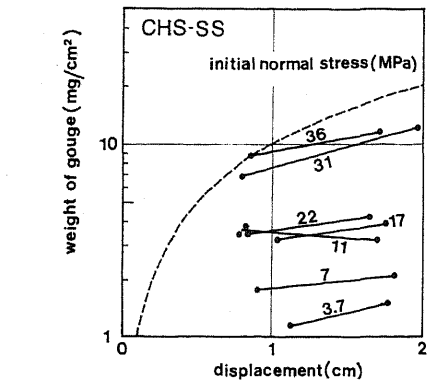

(a)

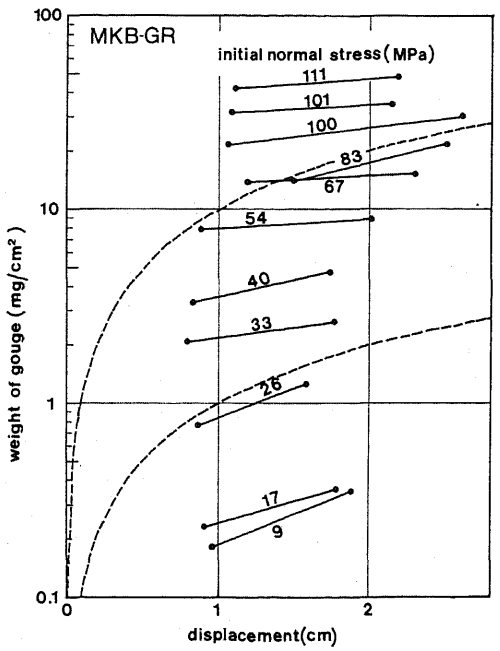

(b)

Fig. 1. The weight of gouge developed per unit area of the sliding surfaces as a function of displacement. The numbers denote the initial normal stress (MPa) immediately before the onset of sliding. Each line corresponds to a cycle which consists of three sliding runs. The datum which shows the larger amount of gouge and the larger magnitude of displacement is obtained as a summation of two sliding runs. The broken lines show the lines which proportionally increase with displacement. (a) Choshi sandstone (CHS-SS), (b) Makabe granite (MKB-GR).

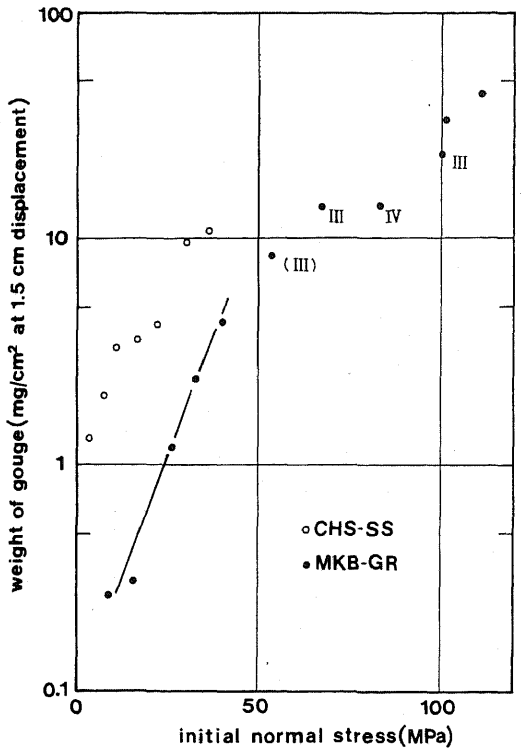

Fig. 2. The relation between the initial normal stress and the weight of the gouge which were developed per unit area and at the same magnitude of displacement (1.5 cm). The Roman numerals denote the representative sliding mode (see text).

strengths of CHS-SS and MKB-GR are about 65 MPa and 150 MPa, respectively.

The larger the magnitude of displacement, the larger the amount of gouge developed (Fig. 1). However, the amount of gouge is not proportional to the magnitude of displacement. The broken lines in Figs. 1 (a) and (b) denote the lines which proportionally increase with displacement. It seems that there exists an upper limit in the gouge productivity due to displacement.

The effect of the normal stress on the productivity of gouge is shown in Fig. 2. As the normal stress becomes larger, the amount of gouge increases. Below the normal stress of 40–50 MPa, the logarithm of the amount of gouge proportionally increases with the normal stress. In the range over 40–50 MPa, however, the increasing rate diminishes in MKB-GR. It should be noted that there exists a change in the productivity of gouge at the normal stress of 40–50 MPa. It will be discussed in light of the surface roughness.

In Fig. 2, the Roman numerals denote the representative mode of sliding (One data point is derived from three sliding runs, the sliding modes of which are not

always the same, so that the representative mode is that of the first or the third run in a cycle). Mode III represents the episodic sliding, which commences as violent stick-slips with considerable magnitude of stress drop and rapidly shifts to a stable sliding or to continuous stick-slips with small stress drop. Mode IV represents the violent stick-slips with large magnitude of stress drop. The data without the numerals are for stable sliding or continuous stick-slips with small stress drop. The sliding modes are characterized by the magnitude of stress drop (YOSHIOKA, 1985). Figure 2 suggests that when the stress drop is large, the amount of gouge decreases. The stress drop or the sliding mode probably affects the productivity of the gouge.

3.2 Particle size distribution

The particle size d_i was measured for the gouge of MKB-GR using a centifigural particle size analyzer (made by Shimadzu Co., Ltd., Japan). Since the analysis requires an amount of gouge more than 100 milligrams, we could not analyze all samples. Table 2 shows a list of the analyzed samples. Figure 3 shows the principle of the analyzer. Its output is a strip chart record showing the intensity of the optical beam which passed through the colloidal suspension of gouge. From the charts, we read the beam intensities corresponding to particle sizes. They are plotted as a thin line graph in the upper part of Fig. 4. Assuming that the maximum particle size is 20 microns in diameter, we calculated the cumulative weight percent p_i, which are also plotted in the upper part of Fig. 4. The thick solid curve $P(x)$ in the upper part of Fig. 4 was computed using a least squares program to fit the plotted data (x_i, p_i), where $x_i = \log d_i$ (for details of the calculation method, see Appendix). The lower part of Fig. 4 shows the derivative of the cumulative curve, which is the particle size distribution $Q(x)$. The curve $Q(x)$ is normalized by its maximum value.

The curve $Q(x)$ is a log-normal distribution which has a peak at about 5 microns (d_m in Table 2), independent of the normal stress. The distribution at smaller diameters than d_m shows various forms. Three examples are shown in Figs.

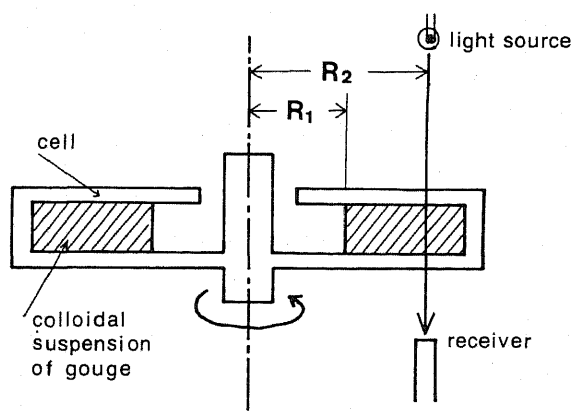

Fig. 3. The principle of the centifigural particle size analyzer. The cell rotates and the gouge precipitates to the outer side. $R_1 = 6$ cm, $R_2 = 8$ cm.

Table 2. A list of the samples used for the particle size analysis.

Cycle (σ_i: MPa)	Run No.	D (cm)	w (g)	w/A (mg/cm^2)	d_m (μm)	S (10^4 cm^2)	S/A (cm^2/cm^2)	S/w (10^4 cm^2/g)	Frac. energy (10^4 erg/cm^2)	E (10^8 erg/cm^2)
6	MKB-16, 17	2.066	0.354	8.85	5.0	0.55	138	1.56	2.8–14	7.4
(54)	MKB-18	0.885	0.315	7.88	4.5	0.46	115	1.46	2.3–12	3.0
7	MKB-19, 20	2.344	0.605	15.1	5.3	0.98	245	1.62	4.9–25	9.4
(67)	MKB-21	1.199	0.546	13.7	5.2	0.82	205	1.50	4.1–21	4.2
8	MKB-22, 23	2.552	0.859	21.5	5.3	1.45	363	1.69	7.3–36	10.6
(83)	MKB-24	1.517	0.558	14.0	5.0	0.79	198	1.42	4.0–20	5.0
9	MKB-25, 26	2.598	0.737	30.2	4.5	1.12	459	1.52	9.2–46	13.6
(100)	MKB-27	1.060	0.532	21.8	4.8	0.71	291	1.33	5.8–29	4.6
10	MKB-28, 29	2.145	0.848	34.8	4.0	1.37	561	1.61	11–56	13.9
(101)	MKB-30	1.086	0.775	31.8	4.3	1.16	475	1.50	9.4–48	6.6
11	MKB-31, 32	2.195	1.177	48.2	5.2	1.68	689	1.43	14–69	12.9
(111)	MKB-33	1.107	1.024	42.0	4.0	1.51	619	1.48	12–62	7.8
—	MKB-34–60	—	—	—	5.3	—	—	—	23–116	—

σ_i, initial normal stress; D, total displacement; w, total weight of gouge; A, sliding surface area; S, surface area of gouge; d_m, diameter which gives the maximum value to $Q(x)$.

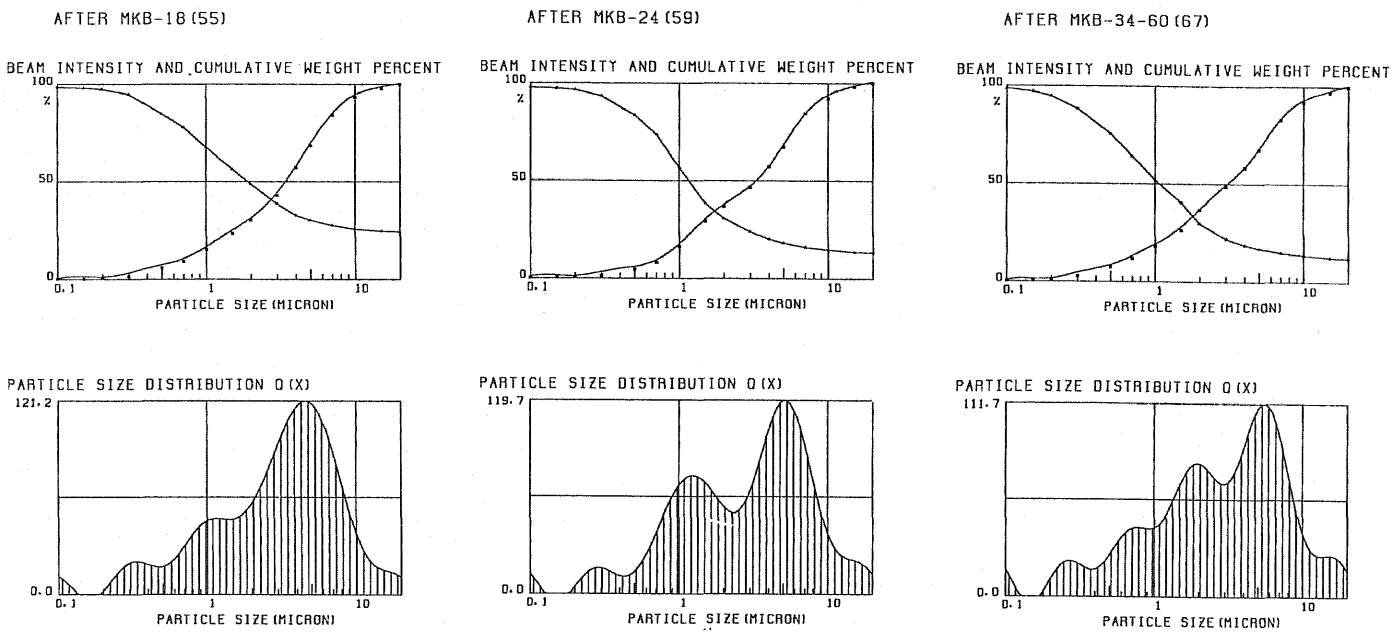

Fig. 4. Particle size distribution of the gouge. Upper: a line graph denotes the intensities of the optical beam which passed through the colloidal suspension of gouge. Plotted data are the cumulative weight percent p_i which are calculated from the beam intensities. The solid curve is a continuous and differentiable function $P(x)$, which is obtained by the least squares method (see Appendix). Lower: the particle size distribution $Q(x)$, which is the derivative of $P(x)$.

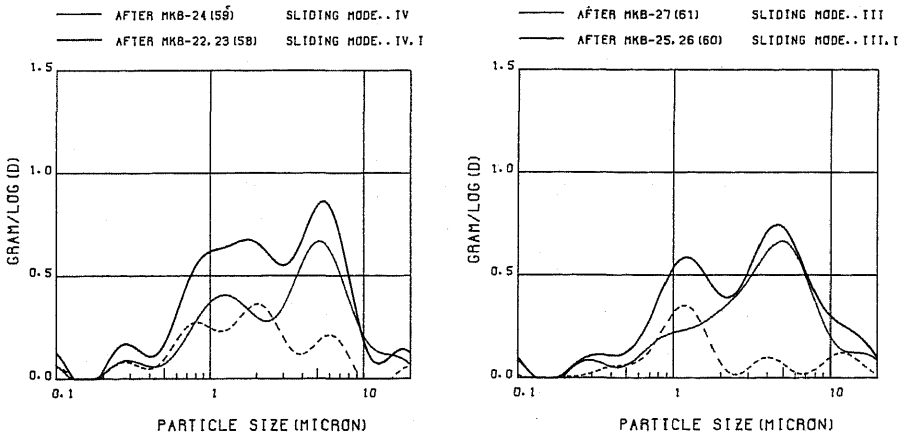

Fig. 5. The effect of the sliding magnitude on the particle size distribution of gouge. The thick and thin solid curves denote the particle size distribution after two sliding runs and one sliding run, respectively. The broken line represents the difference between these two curves.

4(a), (b), and (c). This variation may reflect the sliding behaviour such as displacement magnitude, sliding mode and so on.

One cycle consisted of three sliding runs under the same condition of the initial normal stress: the second run in a cycle was successively carried out following the first run without the removal of gouge, and the third run was after the removal of gouge. The total displacement of the first and second runs is about two times larger than that of the third run. Thus we can estimate the effect of the magnitude of displacement on the particle size distribution by comparing the two particle size distributions with each other in a cycle. Figure 5 shows two examples of the comparison. The thick solid curve denotes the distribution of the gouge obtained after the first and the second runs in a cycle and the thin solid curve denotes that after the third run. Therefore the difference between the two lines represents the displacement effect of the second run, which is shown by the broken line. As shown in Fig. 5, the peak of the broken line does exist at diameters smaller than 5 microns. This fact suggests that the sliding with gouge on the sliding surfaces breaks the gouge developed by the preceding sliding rather than plough the surfaces and create new gouge. This is probably one reason why the amount of gouge is not proportional to the magnitude of displacement. A typical example appeared in the data after MKB-60 (Fig. 4(c)). The slidings from MKB-34 to MKB-60 were successively carried out without the removal of gouge (Table 1). Although the total displacement amounted to about 30 cm, the weight of the gouge developed during the 27 runs amounted only to 1.8 g, which is only 1.7 times as much as that of gouge after only one sliding of MKB-33. Further there seem to be some peaks at smaller diameters in $Q(x)$ of Fig. 4(c). The gouge is likely to become finer with slip,

producing an increase in surface area without an increase in mass. This is still a comminution product. Therefore it would be useful to calculate the surface area of gouge.

The surface area S of gouge can be estimated from the weight of the gouge w and their particle size distribution $Q(x)$. Assuming that the shape of the gouge particles is spherical, S is obtained by the following formula,

$$S=\frac{6w}{\rho}\int\frac{Q(x)}{10^x}\mathrm{d}x\,, \tag{1}$$

where $x=\log d$, d is the diameter of a particle and ρ is the density. The results are shown in Table 2.

In general, the total area of gouge per unit sliding surface, S/A, increases with normal stress. However, this increase in surface area is due to the increase in mass which increases with normal stress, because the surface area per unit mass, S/w, is independent of the normal stress (Table 2).

The effect of displacement magnitude on the surface area appears in the increase in surface area per unit mass in a cycle. In cycle 6, for example, the surface area per unit mass at displacement 0.885 cm is 1.46×10^4 cm^2/g and that at 2.066 cm is 1.56×10^4 cm^2/g. Except for cycle 11, the surface area per unit mass increases with displacement.

4. *Surface Roughness*

The sliding surfaces were ground flat with 800 grit abrasives (the average diameter is about 20 microns) only once before the first run. Therefore, the surface roughness before the experiments did not remain through all series of experiments: the surface roughness varied with the progress of the experiments. Thus we observed the variations of the surface roughness after removal of gouge two times a cycle throughout Series A experiment of MKB-GR.

A needle probe method was used for the observation. Figure 6 shows the traverse lines of the tracer on a sliding surface, which are parallel to the sliding direction. The length of each traverse line was about 2 cm. The outputs from the tracer were amplified by 250 times and fed on a strip chart recorder. Since the speed of the tracer was 0.1 mm/s and the cut-off frequency of the recorder was about 1.0 Hz, the minimum wavelength which could be detected by the observation was about a few 100 microns.

Figure 7 shows some examples of the profiles of the surface roughness. The original chart records have a defect in that the base line (the broken line in Fig. 7) of the records slightly inclined because it was difficult to set the sample horizontally. Therefore the component of the inclination was removed to guide the reader's eye.

Some analytical methods have been used to represent the surface roughness. For example, BARTON and CHOUBEY (1977) used the joint roughness coefficient (JRC) and KUWAHARA *et al.* (1985) analyzed the profiles of the surface roughness

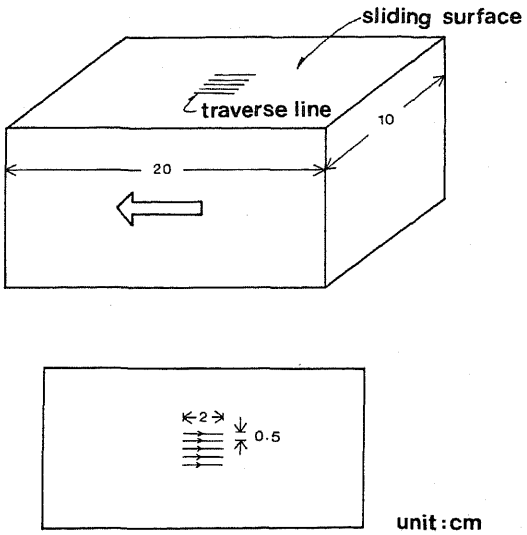

Fig. 6. The traverse lines used to observe the surface roughness. The arrows in the lower figure denote the direction of the tracer.

using the frequency analysis method. In the present study, we used a parameter F to represent the surface roughness. F is defined by

$$L \propto s^{1-F}, \tag{2}$$

where L is the total length measured by a scale of length s. This representation is similar to a definition of the fractal dimension of curves (MANDELBROT, 1983). In that representation, the defect of the records mentioned earlier is negligible. Figure 8 shows an example of L vs. s plot used to determine F. The inclination of the straight line corresponds to $1-F$. The rougher the surface is, the larger the value of F.

Figure 9 shows the variation of F with the normal stress. One data point and its error bar represent the average of F and one standard deviation among the five profiles observed after a run.

F is kept constant or slightly decreases with normal stress in the range less than 40 MPa and rapidly increases at about 40 MPa. We call the stress which gives the discontinuity the critical stress σ_c. In the range over σ_c, F gradually increases with the increase of the normal stress. The ploughing of the surfaces began to occur with long wavelengths (longer than several 100 microns) at σ_c.

Figure 9 suggests another feature of the surface roughness. The open circles denote the sliding mode III or IV, and the closed circles I or II. Out of two data which are under the same initial normal stress condition over 50 MPa, the higher one is after the run whose sliding mode is III or IV. The sliding mode is likely to relate to the surface roughness: after the stick-slips occur with large magnitude of

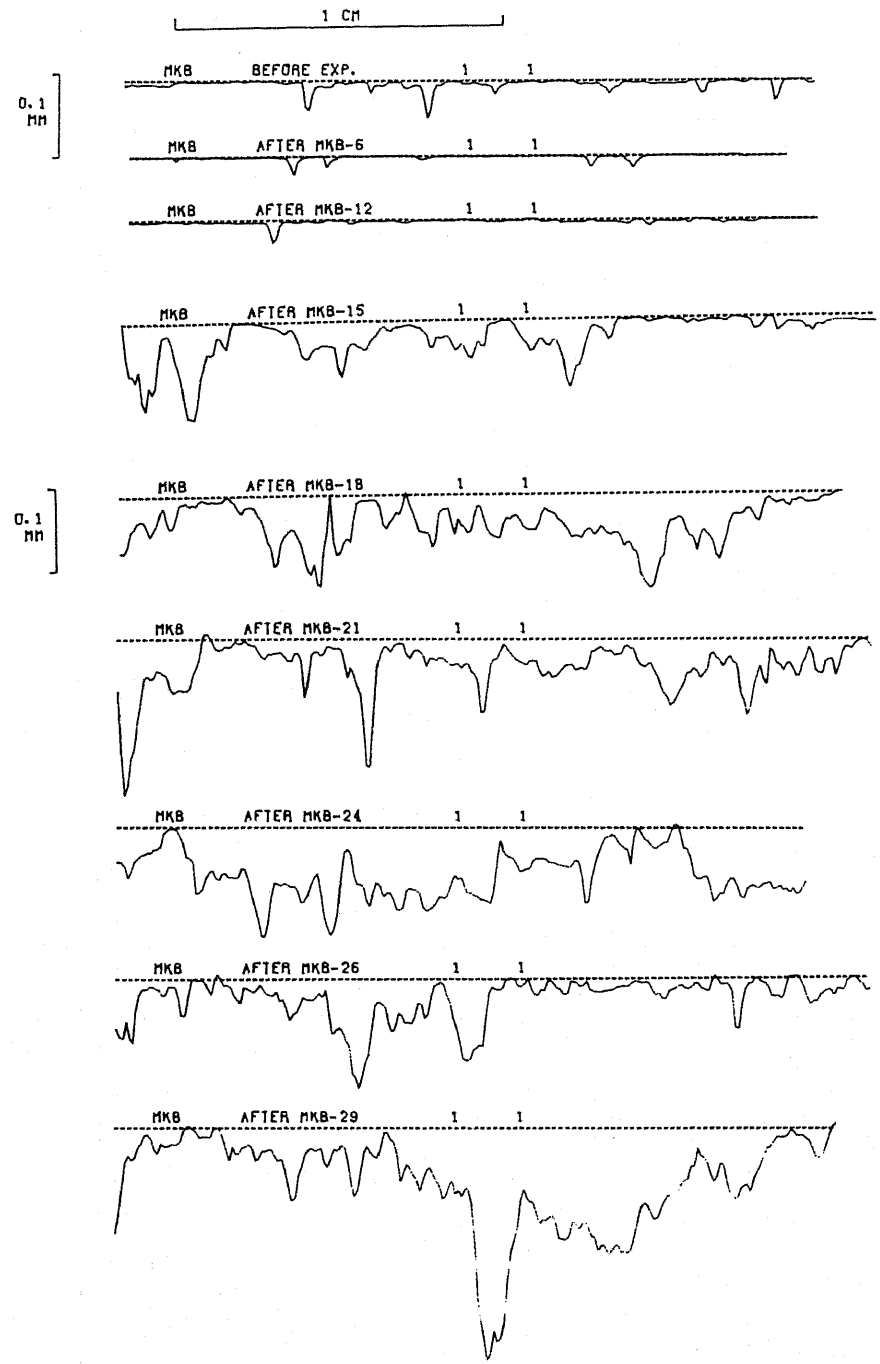
1 CM
MKB BEFORE EXP. 1 1
0.1 MM
MKB AFTER MKB-6 1 1
MKB AFTER MKB-12 1 1
MKB AFTER MKB-15 1 1
MKB AFTER MKB-18 1 1
0.1 MM
MKB AFTER MKB-21 1 1
MKB AFTER MKB-24 1 1
MKB AFTER MKB-26 1 1
MKB AFTER MKB-29 1 1

Fig. 7

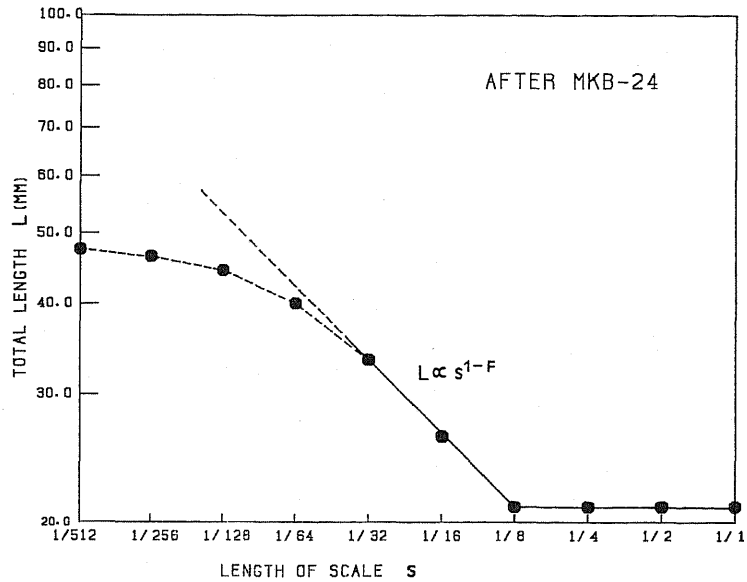

Fig. 8. An example of L vs. s plot used to determine F. The inclination of the solid line is $1-F$.

stress drop (mode III or IV), the surface roughness increases. Since surface roughness is considered to be a result of the sliding process, this experimental result suggests the difference between the sliding processes of stable sliding and stick-slip.

5. *Discussion*

The fracture energy can be estimated by assuming that the surface energy of the rock minerals ranges from 200 to 1,000 erg/cm^2 (BRACE and WALSH, 1962). The calculated fracture energy is shown in Table 2. In the calculation, the area S' which increased on the sliding surfaces due to the ploughing is not taken into account, because S' is easily supposed to be much smaller than S.

The assumption that the gouge particles are spherical may be incorrect. The particles are irregular in shape and their surface area is likely to be about three times as large as that of a sphere (NAKAMURA *et al.*, 1984). If this is the case, the fracture energy in Table 2 must be corrected to be about three times larger.

In Table 2, the total energy E which is supplied by the testing machine per unit sliding area is also shown. The energy E is calculated from both the magnitude of

Fig. 7. Some examples of the profile of the surface roughness. From before the experiment to the run number MKB-12 (the normal stress was less than 33 MPa), the roughness seems not to vary. After MKG-15, however, the violent ploughings of the surface occurred.

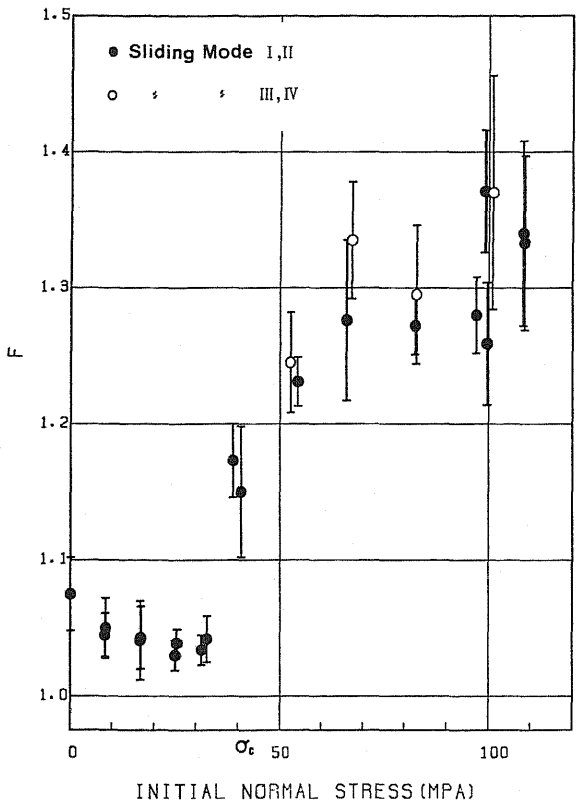

Fig. 9. The variation of the surface roughness in MKB-GR with the increase in normal stress. The open and closed circles represent the sliding mode III or IV and I or II, respectively. The error bars denote one standard deviation among five profiles.

displacement and the average shear stress of the testing machine during sliding. The order of E is 10^8 erg/cm^2, while that of the fracture energy is $10^4 \sim 10^5$ erg/cm^2. The fracture energy occupies only 0.01–0.1% of the total energy E even if we take the irregularity of the particles in shape and the increase of the sliding surfaces due to ploughing into account. This value agrees well with the efficiency of grinding (BOND, 1950).

The energy stored in a loading frame is released when slidings occur in experiments. The released energy will be coverted to the heat energy, the fracture energy and the elastic wave energy. The distribution process of the energy in experiments is similar to that in earthquakes. In our experiments, we observed the temperature variations (YOSHIOKA, 1985), which is used to estimate the heat energy, and the weight and the particle size distribution of gouge, which is used to estimate the fracture energy. The quantitative measurement of the fracture energy shows that the fracture energy which is required to create new surfaces of gouge is very small in

the total energy supplied by the testing machine. Therefore we conclude that the released energy is converted mainly to the two forms of energy: the heat energy and the elastic wave energy.

As shown in the previous paper, the generation of heat depends upon the stress drop $\Delta\tau$; when the ratio of $\Delta\tau$ to the initial stress τ_1 is large, the heat energy is small. The significant part of the released energy is consumed in another form of energy. Thus the residual energy is considered to be consumed in the generation of the elastic waves.

Although the fracture energy occupies only a small part in the distribution of energy, there seems to be a correlation between the gouge and the sliding behaviour or the distribution of energy.

The observations with respect to the gouge and the surface roughness in our experiments are summarized as follows. There exists a critical stress, which is shown by gouge data and especially by surface roughness data. These data suggest a difference in the process of the gouge production between below and over σ_c: below σ_c the gouge is produced by breaking the tips of the asperities, whereas over σ_c by the ploughing of the surfaces. Thus the surfaces are smoothed rather than roughened below σ_c. Figure 10 schematically illustrates the difference. If the intact rock could be distinguished from the short wavelength asperities as shown in Fig. 10, the ploughing of the intact rock could occur only over σ_c.

Below the critical stress, stable slidings or continuous stick-slips with small stress drop occur independently of gouge. On the other hand, the sliding mode depends upon the presence of gouge in the range over the critical stress. The stick-slips with large stress drop will occur if there is no gouge on the sliding surfaces, and after the generation of gouge due to slip, the sliding mode shifts to stable sliding. Since the distribution of energy depends upon the sliding mode, the gouge plays an important role in the energy budget.

The gouge and the surface roughness are not only causes but also effects of sliding behaviour. When we regard gouge and surface roughness as an effect of sliding behaviour, it is suggested that these data reflect the history of sliding and the difference of sliding modes. For example, the surface area of gouge per unit mass increases with displacement, without increase in amount of gouge. Thus the particle size distribution of gouge is an effect of sliding. Further, with respect to sliding modes, after the stick-slips occur with large stress drop, less heat is generated, smaller amount of gouge is developed, and surface roughness becomes larger than after the stable slidings occur. These experimental results would be useful for investigating the source mechanism of earthquakes if compared with fields data.

The gouge and the surface roughness probably play an important role in the sliding process and reflect the history of sliding, although the surface energy of them is very small in the total energy consumed through the sliding process. It is useful to study the variations of gouge and surface roughness in experiments for investigating the earthquake source mechanism.

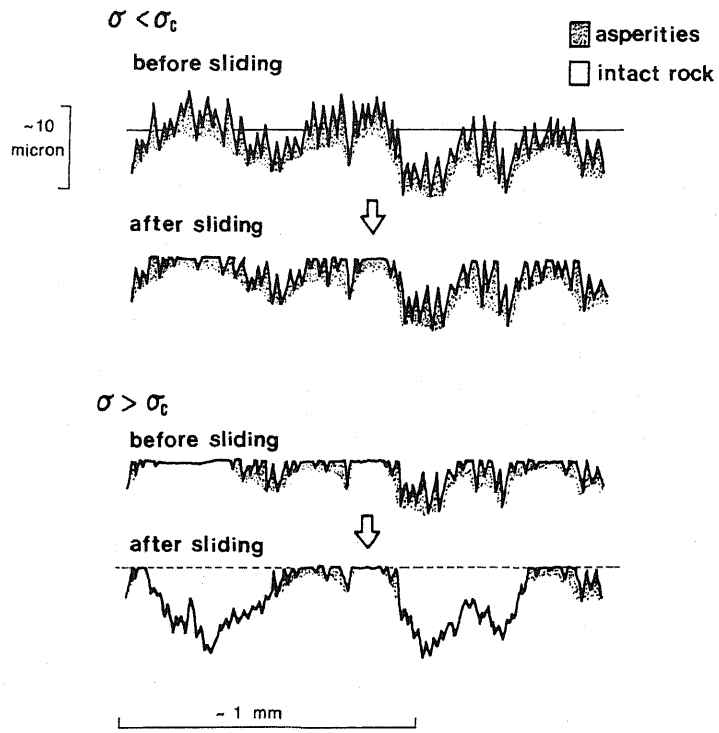

Fig. 10. Schematical illustrations of the sliding surface, before and after sliding. The upper figures are for the stress level below the critical stress σ_c, and the lower over σ_c. The dotted area denotes the part that is asperities and the other area is the part that is the intact rock. The scales denote the orders of length of the vertical and the horizontal axes.

I would like to acknowledge valuable suggestions by Dr. H. Mizutani and Dr. M. Kikuchi. Discussions with Dr. T. Hirasawa, Dr. K. Yamamoto, Dr. M. Ohnaka and Dr. Y. Kuwahara were particularly helpful.

APPENDIX

In order to describe a continuous curve of the particle size distribution, it is necessary to represent the plotted data of the cumulative weight percent by a continuous differentiable function. Let the logarithm of the particle size be x_i, and cumulative weight percent be p_i, where i denotes i-th data. Since the data of the cumulative weight percent, of course, increase with increasing the particle size, we take an inclined straight line from (x_1, p_1) to (x_N, p_N) as a base line, where N denotes the total number of data. The straight line is expressed as

$$p=\frac{p_N-p_1}{x_N-x_1}(x-x_1)+p_1\,. \tag{A.1}$$

Let the difference between the plotted data p_i and the straight line at $x=x_i$ be y_i. The difference y_i is expressed as

$$y_i=p_i-\left\{\frac{p_N-p_1}{x_N-x_1}(x_i-x_1)+p_1\right\}. \tag{A.2}$$

We apply the following method to the data (x_i, y_i).

An arbitrary continuous and differentiable function $f(x)$ can be expressed as

$$f(x)=a_0+\sum_{n=1}^{\infty} a_n\cdot\cos nx+\sum_{n=1}^{\infty} b_n\cdot\sin nx\,. \tag{A.3}$$

If the summation converges, an approximation of (A.3) is given by the finite summation as

$$f(x)=a_0+\sum_{n=1}^{m} a_n\cdot\cos nx+\sum_{n=1}^{m} b_n\cdot\sin nx\,. \tag{A.4}$$

Since the terms in the right-hand side of (A.4) have the orthogonal relation with each other in the interval $0\leqq x\leqq 2\pi$, the coefficients $a_0, a_1, a_2, \cdots, b_1, b_2, \cdots$ can be independently determined. Therefore, using a least squares method, a_0 is determined as

$$a_0=\frac{1}{N}\sum_{i=1}^{N} y_i\,. \tag{A.5}$$

Similarly, a_n and b_n are given by

$$\begin{aligned}
a_n&=\left[\sum_{i=1}^{N} g_i^{m-1}\cdot\cos\delta_i^n\cdot\sum_{i=1}^{N}\sin^2\delta_i^n-\sum_{i=1}^{N} g_i^{m-1}\cdot\sin\delta_i^n\cdot\sum_{i=1}^{N}\sin\delta_i^n\cdot\cos\delta_i^n\right]\Bigg/\\
&\qquad\left[\sum_{i=1}^{N}\sin^2\delta_i^n\cdot\sum_{i=1}^{N}\cos^2\delta_i^n-\left(\sum_{i=1}^{N}\sin\delta_i^n\cdot\cos\delta_i^n\right)^2\right],\\
b_n&=\left[\sum_{i=1}^{N} g_i^{m-1}\cdot\sin\delta_i^n\cdot\sum_{i=1}^{N}\cos^2\delta_i^n-\sum_{i=1}^{N} g_i^{m-1}\cdot\cos\delta_i^n\cdot\sum_{i=1}^{N}\sin\delta_i^n\cdot\cos\delta_i^n\right]\Bigg/\\
&\qquad\left[\sum_{i=1}^{N}\sin^2\delta_i^n\cdot\sum_{i=1}^{N}\cos^2\delta_i^n-\left(\sum_{i=1}^{N}\sin\delta_i^n\cdot\cos\delta_i^n\right)^2\right],
\end{aligned} \tag{A.6}$$

where

$$\delta_i^n=2\pi n\frac{x_i-x_1}{x_N-x_1} \tag{A.7}$$

and

$$g_i^{m-1}=y_i-f_{m-1}(x_i)\,. \tag{A.8}$$

Thus the approximate cumulative function of the weight percent $P(x)$ is expressed as

$$P(x)=\frac{p_N-p_1}{x_N-x_1}(x-x_1)+p_1+a_0+\sum_{n=1}^{m}\{a_n\cdot\cos\delta^n+b_n\cdot\sin\delta^n\}\,,\quad x_1\leqq x\leqq x_N\,, \tag{A.9}$$

where $\delta^n=2\pi n(x-x_1)/(x_N-x_1)$. The particle size distribution $Q(x)$, which is the derivative of (A.9) with respect to x, is given by

$$Q(x)=\frac{p_N-p_1}{x_N-x_1}+\sum_{n=1}^{m}\frac{2\pi n}{x_N-x_1}\{-a_n\cdot\sin\delta^n+b_n\cdot\cos\delta^n\}\,. \tag{A.10}$$

REFERENCES

BARTON, N. and V. CHOUBEY, The shear strength of rock joints in theory and practice, *Rock Mech.*, **10**, 1–54, 1977.

BOND, F. C., A new theory of comminution, *Min. Eng.*, **187**, 871–878, 1950.

BRACE, W. F. and J. B. WALSH, Some direct measurements of the surface energy of quartz and orthoclase, *Am. Mineral.*, **47**, 1111–1122, 1962.

ENGELDER, J. T., Microscopic wear grooves on slickensides: Indicators of paleoseismisity, *J. Geophys. Res.*, **79**, 4387–4392, 1974.

HUSSEINI, M. I., Energy balance for motion along fault, *Geophys. J. R. Astron. Soc.*, **49**, 699–714, 1977.

KING, C., Seismic efficiency, *J. Geophys. Res.*, **74**, 1702–1703, 1969.

KUWAHARA, Y., M. OHNAKA, K. YAMAMOTO, and T. HIRASAWA, The relation between the profiles of fault surfaces and the faulting process in stick-slip, *Prog. Abstr. Seismol. Soc. Jpn.*, No. 1, p. 222, 1985 (in Japanese).

LOCKNER, D. A. and P. G. OKUBO, Measurements of frictional heating in granite, *J. Geophys. Res.*, **88**, 4313–4320, 1983.

MANDELBROT, B. B., *The Fractal Geometry of Nature*, W. H. Freeman and Company, New York, 1983.

NAKAMURA, H., K. ITOH, and J. MATSUDA, The measurement of surface area in fragments. A discussion for K_r absorption method, *Prog. Abstr. Seismol. Soc. Jpn.*, No. 2, p. 119, 1984 (in Japanese).

OHNAKA, M., Frictional characteristics of typical rocks, *J. Phys. Earth*, **23**, 87–112, 1975.

SCHOLZ, C. H., P. MOLNAR, and T. JOHNSON, Detailed studies of frictional sliding of granite and implications for earthquake mechanism, *J. Geophys. Res.*, **77**, 6392–6406, 1972.

SHIMAMOTO, T., Effects of fault-gouge on the frictional properties of rocks: An experimental study, Ph. D. thesis, Texas A&M Univ., 1977.

SHIMAMOTO, T. and J. M. LOGAN, Effects of simulated clay gouges on the sliding behavior of Tennessee sandstone, *Tectonophysics*, **75**, 243–255, 1981.

SUMMERS, R. and J. BYERLEE, A note on the effect of fault gouge composition and the stability of frictional sliding, *Int. J. Rock Mech. Min. Sci.*, **14**, 155–160, 1977.

WANG, C., N. MAO, and F. T. WU, Mechanical properties of clays at high pressure, *J. Geophys. Res.*, **85**, 1462–1468, 1980.

WU, F. T., L. BLATTER, and H. ROBERSON, Clay gouges in San Andreas Fault system and their possible implications, *Pure Appl. Geophys.*, **113**, 87–95, 1975.

YOSHIOKA, N., A method for estimating the shear stress distribution from temperature measurements during sliding of rocks, *J. Phys. Earth*, **32**, 1–12, 1984.

YOSHIOKA, N., Temperature measurement during frictional sliding of rocks, *J. Phys. Earth*, **33**, 295–322, 1985.